Green Chemistry

PAPER

View Article Online
View Journal | View Issue

Check for updates

Cite this: *Green Chem.*, 2021, **23**, 6527

Chitosan nanocrystals synthesis *via* aging and application towards alginate hydrogels for sustainable drug release†

Tony Jin, ‡[a] Tracy Liu,‡[a] Shuaibing Jiang,[b] Davis Kurdyla,[c] Brittney A. Klein,[d] Vladimir K. Michaelis,[d] Edmond Lam,*[c] Jianyu Li*[b] and Audrey Moores*[a,e]

Received 7th May 2021,
Accepted 26th July 2021

DOI: 10.1039/d1gc01611c

rsc.li/greenchem

Marine biomass waste is a remarkable source of functional molecules and materials. Yet material extraction, conversion and processing are often chemically intensive, preventing the widespread and clean use of these abundant resources for high-end applications. Moreover, current challenges in biomedicine call for the design of novel materials with better functional and mechanical properties. Herein, we present a novel chemical process to afford chitosan nanocrystals (ChsNCs), which uniquely combine a high degree of deacetylation, rod shape and high crystallinity for mechanical robustness. This method is a simple solid-state aging process starting from chitin nanocrystals (ChNCs) and requiring limited chemical and energetic input, which we have quantified using process mass intensity as the sustainability metric. This method, as well as a previously reported solution-based method, afforded a family of novel nanomaterials, which we used to form alginate hydrogels. The resulting materials are the first examples of ChsNC-based hydrogels and featured superior performances in terms of both rheological properties, as well as sustained drug release, as compared to previously reported chitosan/alginate systems. This work opens an avenue for functional soft materials using a green resource *via* a clean process.

Published on 29 July 2021. Downloaded on 4/8/2026 1:39:49 PM.

Introduction

The study of hydrogels has been a subject of intense research, with advancements in a diverse variety of fields such as tissue engineering,[1] microfluidic devices,[2] adhesives,[3] agriculture,[4] catalysis,[5] drug delivery,[6] and bone scaffolding materials.[7] The ability for these hydrophilic 3D polymeric structures to swell in water and biological fluid makes them mimics of natural tissue, endowing them with incredible applications.[8–10] Notably, cellulose and chitin, are respectively the first and second most abundant biopolymers in the world. As such, these biopolymers have been intensely focused on as both hydrogel[9–12] and aerogel[13] components due to their bioavailability and biocompatibility.[14–16] Chitin is particularly interesting because its deacetylation affords chitosan, which uniquely possesses a primary amine functionality on the C2 unit of its glucose backbone.[15] The degree of deacetylation (DDA) is a common unit to measure the proportion of primary amines to acetamide functionalities, with chitin and chitosan possessing <15% and >70% DDA, respectively.[17] In chitosan, once the primary amine becomes quaternary and bears a positive charge below pH 6.3, it can readily form hydrogels with negatively charged crosslinkers and co-monomer units.[18] Additionally, chitosan also possesses antibacterial and antioxidant capabilities due to its inherent positive charge, making it capable of penetrating negatively-charged cell membranes in bacteria.[19,20] Through these advantages, chitosan use has become increasingly prevalent in biomedicine.[21]

Chitin and chitosan extraction from natural sources is however not a perfect process, plagued as it is by its reliance on harsh chemical conditions. In particular, chitin deacetylation into chitosan typically relies on the use of corrosive alkaline solutions, heated at high temperatures for extensive periods and ultimately generates toxic effluents.[22] Yet, chitin

[a]Department of Chemistry, McGill University, 801 Sherbrooke St West, Montreal, Quebec, H3A 0B8, Canada. E-mail: audrey.moores@mcgill.ca
[b]Department of Mechanical Engineering, McGill University, 817 Sherbrooke St West, Montreal, Quebec, H3A 0C3, Canada. E-mail: jianyu.li@mcgill.ca
[c]Aquatic and Crop Resource Development Research Centre, National Research Council of Canada, 6100 Royalmount Avenue, Montreal, Quebec, H4P 2R2, Canada. E-mail: edmond.lam@cnrc-nrc.gc.ca
[d]Department of Chemistry, University of Alberta, 11227 Saskatchewan Dr., Edmonton, Alberta T6G 2G2, Canada
[e]Department of Materials Engineering, McGill University, 3610 University Street, Montreal, Quebec H3A 0C5, Canada

†Electronic supplementary information (ESI) available: Details of experimental procedures and further supporting figures and schemes – PDF. See DOI: 10.1039/d1gc01611c

‡These authors have contributed equally to the published work.

Published on 29 July 2021. Downloaded on 4/8/2026 1:39:49 PM.

and chitosan are sourced from crustacean shell waste, which is produced in the multi-million-ton scale every year and is mostly discarded resulting in a negative environmental impact, despite their obvious chemical value.[23–28] Several innovative strategies have focused on improving the extraction, purification and transformation methods, taking advantage of alternative processes such as ionic liquids,[29] glycerol,[30] biocatalysts,[31] or mechanochemistry.[32–34]

In order to further valorise these biopolymers into high-end applications, researchers have explored their extraction as nanocrystallites *via* a partial depolymerization procedure; raw cellulose or chitin can be transformed into cellulose nanocrystals (CNCs) and chitin nanocrystals (ChNCs), respectively.[35–39] These materials feature high aspect ratios and high crystallinity.[40] CNCs in particular have been the focus of intense research attention in the last two decades and have been applied to a wide range of sectors, from coatings to catalysis and biomedicine.[41–43] These nanomaterials have also been applied to the formation of hydrogels, where they typically bring about enhanced mechanical durability for applications in scaffolding materials and drug delivery.[44–46] For such applications, the crystallinity, morphology, and size of the nanocrystal are key features. For instance, CNCs have the ability to augment the mechanical properties of the resulting composite, from the combining effect of their crystallinity and their rod shape.[47–49] For instance, Yang *et al.* described that CNCs with higher aspect ratios conferred improved mechanical stability to poly(acrylamide) hydrogels.[50] Yet, CNCs lack naturally occurring functional groups enabling direct covalent or ionic crosslinking, so they are typically incorporated inside the hydrogel matrix by physical mixing.[9] There are instances of CNCs being able to interact and bind with the gelling matrix, yet this requires surface modification of the CNCs with more treatment steps, further complicating the fabrication of such reinforcement materials.[51,52] ChNC, on the other hand, have been less studied. Huang *et al.* used ChNCs with a 10% DDA as a reinforcing material for an alginate-based hydrogel with Ca^{2+} as the primary crosslinker.[45] Petrova *et al.* took one step further and used ChNCs with DDA of 30% and alginate together with no Ca^{2+} in acidic media to form hydrogels, which exhibited enhanced mechanical properties and allowed sustained drug release of tetracycline as a model small molecule drug.[53] In these works, the authors emphasized the importance of the presence of amine groups, even at low density, on the surface of ChNCs as a key parameter to allow gelation of the system. In this context, the fabrication of hydrogels from rod-shaped chitosan nanocrystals (ChsNCs) would be ideal. On the one hand, ChsNCs feature positive charges on their surface, which can crosslink with monomers such as alginates. In the context of drug release these positive charges may also be useful to partially bind negatively charged drugs (for instance proteins), to favour slower release. On the other hand, ChsNC with rod-shape and high crystallinity can impart improved mechanical properties to the resulting hydrogel. Until recently though, the synthesis of such ChsNCs had remained elusive, explaining the lack of report of their use as co-substituents in hydrogel composites to this date.

Initial studies of the deacetylation of ChNC resulted in the destruction of their nanocrystalline structure and rod shape, to yield highly deacetylated chitosan "webbed nanoscaffold" (aqueous 40% w/v NaOH at 120 °C for 7 h) (Scheme 1).[54] The Hsieh group explored a much milder approach of basic media deacetylation at lower temperature (50 °C), which successfully retained the nanorod morphology and crystallinity, yet only provided a DDA of ChNCs of up to 40%, affording what they called a core–shell chitin-chitosan nanocrystal.[55,56] Our group reported last year the first method able to access ChsNC with high DDAs and rod shape, while their crystallinity was significantly dropped. This solvo-thermal process enabled the transformation of ChNCs into ChsNCs ($ChsNC^{ST}$), using catalytic amounts of $NaBH_4$ to prevent excessive depolymerization and to preserve their rod shape.[57]

Herein, we report a simple and sustainable aging process to access a new type of ChsNC material ($ChsNC^{Ag}$), featuring a rod shape, good DDAs and high crystallinity from ChNCs. This solvent-free method takes inspiration from past work in our group on the use of aging for the conversion of bulk chitin into bulk chitosan.[33] We used sustainability metrics including process mass intensity (PMI) and established that this novel method cuts the PMI by more than half, as compared to the $ChsNC^{ST}$ synthesis, as well as to other methods in the literature. Then, we studied the resulting family of ChsNC materials, the ones made solvothermally ($ChsNC^{ST}$)[57] and the ones made by aging ($ChsNC^{Ag}$), as cross linkers to afford the first reported nanochitosan-based hydrogels. Comparing $ChsNC^{ST}$ and $ChsNC^{Ag}$ in this context allowed to assess the role of DDA and crystallinity into hydrogel properties. With a Ca^{2+}-free alginate hydrogel formulation, we explored their rheological properties. $ChsNC^{Ag}$ in particular provided superior gelation behaviour, affording a stable gel in half an hour with storage modulus values up to 2 orders of magnitude in comparison with ChNC and $ChsNC^{ST}$. A protein-drug release study was performed with $ChsNC^{Ag}$ or $ChsNC^{ST}$ in Ca^{2+}-cross-linked alginate hydrogels, and showed that $ChsNC^{ST}$ provided prolonged drug release in the time scale of days, unlike other alginate-based gels which tend to release drugs in the matter of hours.[58,59]

Results and discussion

Aging-based synthesis of chitosan nanocrystals ($ChsNC^{Ag}$)

We first sought to develop a synthetic method to access ChsNC with the following properties: (1) high DDA values, (2) crystallinity retention, and (3) rod-like morphology retention, and turned to solid-state, mechanochemical/aging methods as a framework. The Yan and Kerton groups had demonstrated that high-energy milling methods are able to break chitin crystallinity, making it more accessible for deacetylation, and at the same time favour accelerated hydrolysis of its β-1,4-glycosidic linkages.[60] These procedures afforded low MW chitosans,[34]

 This journal is © The Royal Society of Chemistry 2021

Published on 29 July 2021. Downloaded on 4/8/2026 1:39:49 PM.

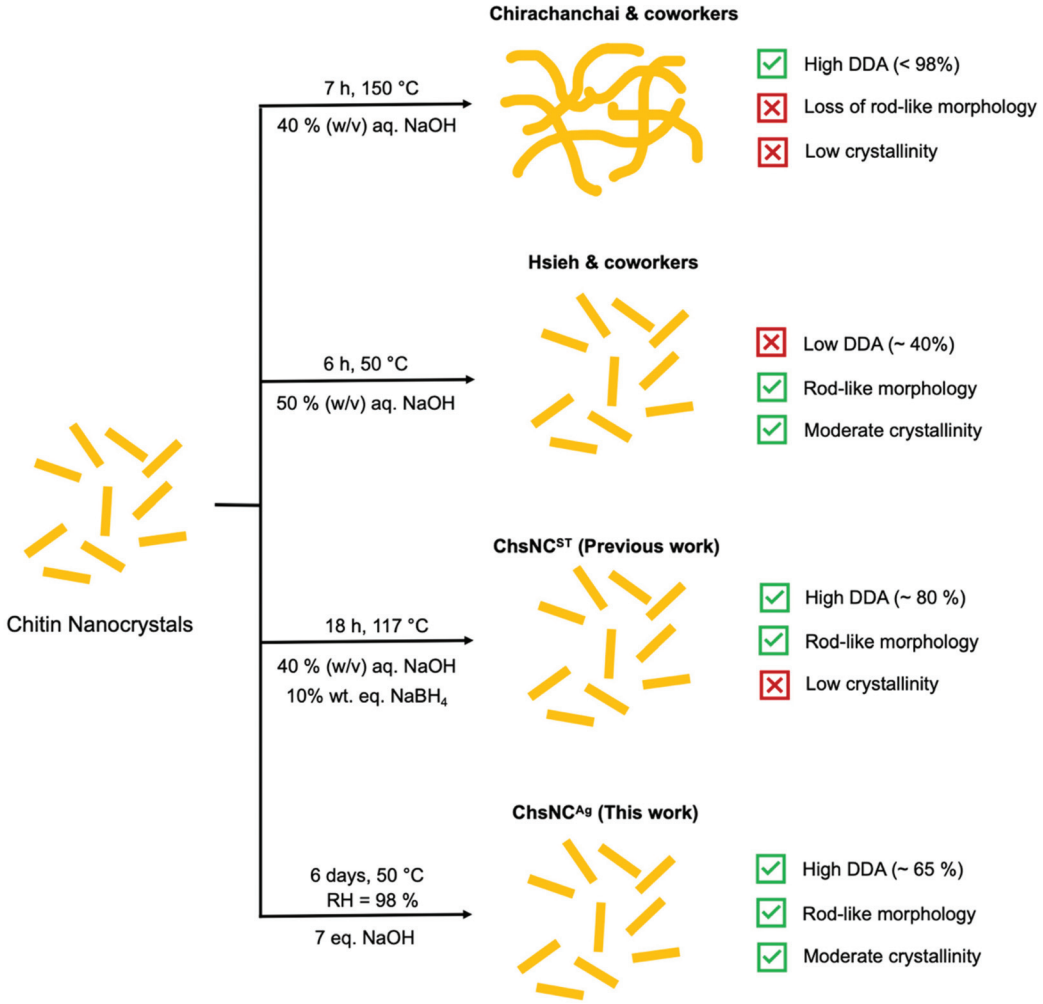

Scheme 1 Current paths towards deacetylation of ChNCs into ChsNCs.

soluble *N*-acetyl-glucosamine oligomers, *N*,*N*′-diacetylchitobiose dimers, as well as *N*-acetylglucosamine monomers.[60,61] Conversely, our group has developed mild mechanochemical methods for the functionalization of polymers while preserving their structural integrity,[62,63] as exemplified with the deacetylation of chitin to yield high MW chitosan.[33] This method relied on three steps, the first one being optional: (1) milling in a vibrational mill to amorphize chitin alone followed by (2) a 5 min milling with NaOH powder and (3) solid-state aging under 98% humidity, with optional heating to 50 °C.[64] The entire process was mild enough to prevent hydrolysis while affording excellent DDA in the 80–95% region.

In this context, we sought to investigate the use of vibrational milling and aging under 98% humidity for the transformation of ChNC into ChsNC. We reasoned that the low depolymerization observed with these methods was conducive to the preservation of nanostructure of the material. We first vibrationally milled ChNCs with either 1 or 2 eq. of NaOH (w/w%) in a 10 mL zirconia milling jar with one 10 mm zirconia ball for 5 min. In another set of experiments, we ground ChNCs in a mortar and pestle under the same conditions. We calculated DDA values through $^{13}C\{^{1}H\}$ multiple-CP/MAS solid-state nuclear magnetic resonance (ssNMR) spectroscopy using an established method previously reported.[65] DDAs of only 2 to 3% were measured in all cases, consistent with our past report on bulk chitin (Fig. S1†).[33] This treatment was however successful in creating a homogeneous powder mixture of the ChNC and NaOH. We thus used this mixture as the starting point for aging experiments, consisting of an incubation period in a closed chamber with a high relative humidity (RH) of 98% at 50 °C and followed the reaction between 12 h and 10 days (Fig. 1a).

DDA was measured along the way by ssNMR and found that it increased steadily from 8.7% at 12 h to 65% at 6 days (Fig. 1b and Table S1†), as seen by the decrease in integral area of both the methyl (~23 ppm) and carbonyl carbon (~177 ppm) associated with the acetylamine functionality is seen (Fig. S2†). After 6 days, the reaction plateaued. The resulting material, hence accessed by aging, was denoted ChsNC^{Ag}. As a matter of comparison, the ssNMR spectra of starting

Published on 29 July 2021. Downloaded on 4/8/2026 1:39:49 PM.

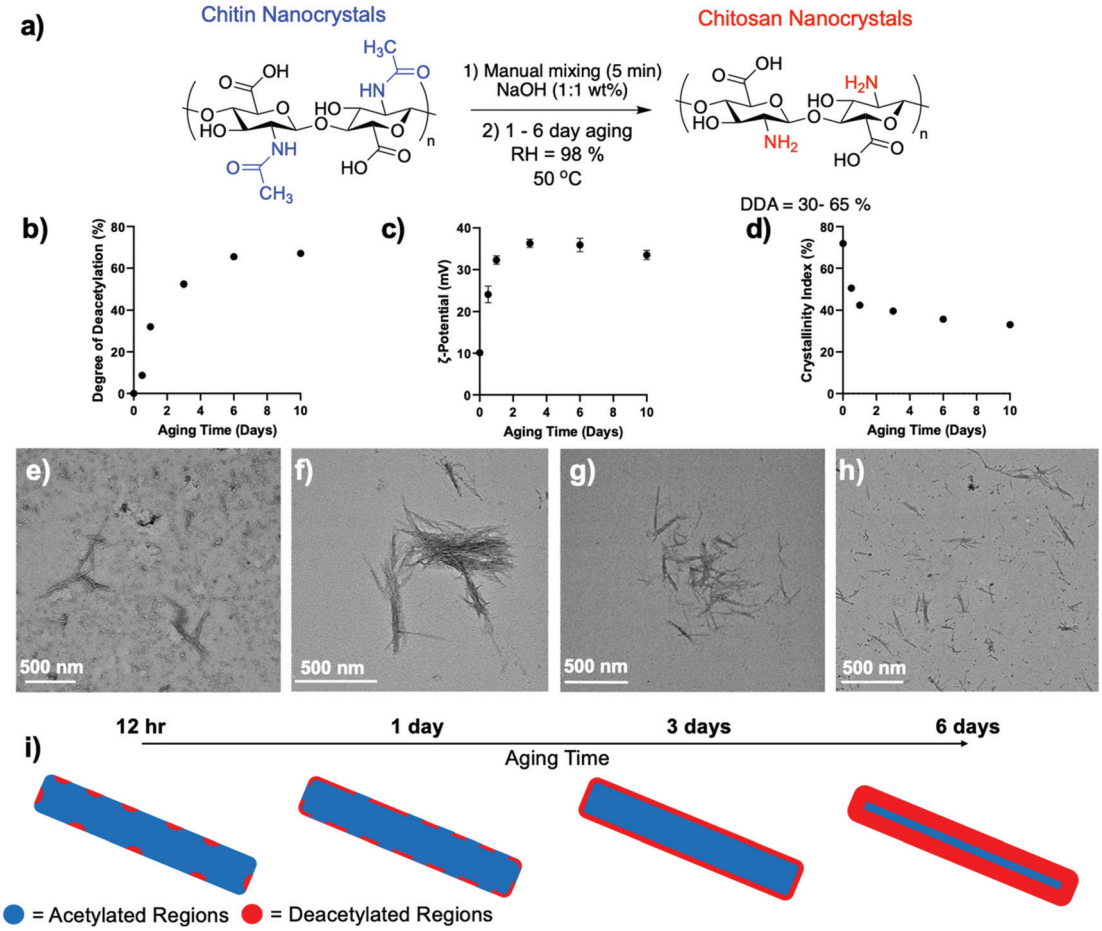

Fig. 1 (a) Schematic depicting the aging reaction parameters for the deacetylation of ChNCs into ChsNCs. (b) DDA, (c) ζ-potential at pH 5 and (d) crystallinity index (CRI) as a function of aging time using the reaction conditions listed in (a). The data shown at 0 aging time is the initial ChNC used without aging. The tabulated values can be seen in Table S1.† Representative TEM image of (e) 12 h aged, (f) 1-day aged, (g) 3-day aged and (h) 6-day aged ChsNCs^{Ag}. (i) Schematic depicting the theorized formation of deacetylated regions on the ChNC over the course of the aging period from 12 h to 6 days, with total deacetylation of the surface starting at 3-day aged ChsNC^{Ag} and further interior deacetylation at 6-day aging time.

material ChNCs and solvo-thermally prepared ChsNCST are provided as Fig. S3,† confirming DDA values of 0% and 88% respectively.

It is important to note, that the DDA value calculated from ssNMR accounts for the entire material, reporting the state of both the surface of the nanocrystals and its core. We thus turned to dynamic light scattering (DLS) of ChsNC^{Ag} aqueous suspensions at pH 5 as a method to track the surface functionalization along the reaction, *via* the measurement of the ζ-potential (Fig. 1c). No matter the aging time, all ChsNC^{Ag} featured ζ-potential values in the positive range, from +24 to +37 mV, indicative of the presence of quaternary ammonium cations – and successful deacetylation. A comparison is made with a suspension of ChNCs, which is the sample at aging day = 0, in which a ζ-potential value of +10.1 mV was observed (Table S1†). Similar to DDA, the ζ-potential values increased as a function of aging time. Yet, while DDA values plateaued at 6 days, the ζ-potential values plateaued and receded slightly from 3 days of aging time onwards. We hypothesize that ChsNC^{Ag} reached a "saturated" level of deacetylation at 3 days, corresponding to the functionalities at the surface of the nanocrystal. From 3 to 6 days, subsequent deacetylation did not affect the surface charge of the particle.

ChsNC^{Ag} samples were further studied by powder X-ray diffraction (pXRD) to measure their crystallinity index (CrI) throughout the aging process. In line with both the DDA and ζ-potential, the CrI of ChsNC^{Ag} dropped rapidly from 72% for ChNC to 51% after 12 h of aging and finally reached 40% and 36% after 3 and 6 of aging, respectively (Fig. 1d). In contrast, ChsNCST featured a lower CrI of 24% (Fig. S4 and Table S1†). The ssNMR is also consistent with the loss in crystallinity in ChsNCST as compared to ChsNC^{Ag}, as revealed by the broadened peaks in Fig. S3.† This broadening is indicative of structural disorder at both the local and medium range. This suggests that loss of crystallinity and deacetylation work in tandem, which has been seen for bulk chitin to chitosan conversion as well as in the nanoscale.[33,57,66]

Finally, the morphology of the nanocrystals was carefully monitored using transmission electron microscopy (TEM) and scanning electron microscopy (SEM, Fig. S5†). No matter the

 This journal is © The Royal Society of Chemistry 2021

Published on 29 July 2021. Downloaded on 4/8/2026 1:39:49 PM.

aging time, ChsNC^{Ag} retained its original rod-like structure – even with longer aging time, as demonstrated by both TEM and SEM (Fig. 1e–h and S5†). The length of the nanorods was measured manually through multiple TEM micrographs (Fig. S6†). The 12 h aged ChsNC^{Ag} had a length of 186 ± 42 nm, the 1-day aged ChsNC^{Ag}, 208 ± 33 nm, the 3-day aged ChsNC^{Ag}, 198 ± 44 nm, and the 6-day aged ChsNC^{Ag}, 203 ± 36 nm. In comparison, the starting ChNCs had an original length of 239 ± 7 nm. We thus observed a small but statistically relevant drop in average length from 239 for ChNCs to a range between 186 and 208 nm for ChsNC^{Ag}. The standard deviation goes from 7 nm for ChNCs to around 40 nm for aged samples. This data is consistent with mild depolymerisation, occurring from the rod tips inwards at the onset of the reaction, under basic conditions and concurrently to deacetylation. Upon comparing various aging times, we noted no clear trend for the observed average rod lengths. For example, the 3-day aged ChsNC^{Ag} had a lower "average" length (198 nm) than the 1-day aged ChsNC^{Ag} (208 nm). Since all ChsNC^{Ag}'s lengths range from 186 and 208 nm with standard deviation around ± 40 nm, we concluded that the observed changes were small and not statically relevant; thus depolymerisation was not significant after the first 30 min of aging. Finally, upon comparison with the solvo-thermal synthesis of ChsNCST, an average length of 182 ± 2 nm was measured, which clearly indicated partial hydrolysis occurring as well.

It is interesting to note that the traditional solvo-thermal basic conditions used to deacetylate bulk chitin are also leading to chitin depolymerisation. In our past work on mechanochemical and aging based chitin deacetylation, we have demonstrated that solvent free conditions enable to greatly limit this depolymerisation.[33] The aging based synthesis of ChsNC^{Ag} reported here is another example of this effect, as we observed little depolymerisation in the form of nanocrystal length shortening. This property is key in being able to retain the crystallinity and shape of the nanocrystals. In the case of the ChsNCST, a similar outcome is achieved in the solution-based method (ChsNCST) by the use of an additive, $NaBH_4$.[57] Interestingly, the reported aging process used to synthesize ChsNC^{Ag} afforded a good level of depolymerisation control without any need for additives, which is a clear difference with the solvent based synthesis of ChsNCST.

Based on the results from these different characterisation methods during the aging process, we can hypothesize that amorphization occurs rapidly, as a consequence of aging in the presence of NaOH. This is accompanied by deacetylation, occurring preferably at the surface of the nanocrystal, which slowly becomes fully saturated over 3 days, as seen in ζ-potential measurements. Next, deacetylation of the deeper structures of the nanocrystal occurred up until a certain threshold, after which the crystalline interior of the nanocrystal is too obstructed to be deacetylated (Fig. 1i).

Sustainability metrics

To summarize, we have proven through a combination of TEM, XRD, ssNMR and ζ-potential measurement techniques that the aging methodology successfully creates ChsNCs with moderate crystallinity, a rod-like shape, and high DDA. While solid-state aging reactions align with green chemistry principles in theory, quantification of such claims must always be done in order to truly provide metrics for comparison with other techniques. Indeed, quantification of aging reactions for chitin have already been reported from our group, and is seen to yield very efficient energy consumption per gram of product (J g^{-1}) in our previous report.[33] Therefore, we look towards quantifying the process mass intensity (PMI) for the transformation of chitin to ChNC and ChNC to ChsNC, as well as a cumulative mass intensity (MI) for four routes (Table 1). The MI was calculated as following the best practices for sustainability metrics,[67] using the following equation:

$$\mathrm{MI} = \frac{\sum \text{total mass of process}}{\text{mass of isolated product}}. \quad (1)$$

We compare our novel aging method to our previously reported solvo-thermal method, as well as other deacetylation methods reported by the Hsieh group and Chirachanchai groups, as outlined in Scheme 1.

The Chirachanchai and co-workers process (Table 1, entry 1) has a lower MI than the one of the Hsieh group (Table 1, entry 2), both for chitin to ChNC conversion and the deacetylation to ChNC to ChsNC. Importantly, the process of Chirachanchai did not retain nanorod morphology of the ChsNCs. In contrast, our previous solvothermal synthesis (Table 1, entry 3) has a PMI of 70.7 for the first step, almost a 4-fold decrease compared to both Chirachanchai and Hsieh methods. This is presumably due to the increased scale of our group's procedure for the synthesis ChNCs (14 g product yield) as opposed to the 5 g product scale of Hsieh method. This is also the case for the drastic difference in PMI for the ChNC to

Table 1 Process mass intensity calculations for four different processes to make ChsNCs starting from chitin

Entry	Deacetylation method	PMI (chitin to ChNC)	PMI (ChNC to ChsNC)	Total MI (chitin to ChsNC)
1	Solvo-thermal base treatment (Chirachanchai group)[54]	246.5	362.5	441.8
2	Mild solvo-thermal base treatment (Hsieh group)[55]	281.9	920	789.3
3	Solvo-thermal base treatment with $NaBH_4$ (previous work)[57]	70.7	377.7	494.4
4	Aging reactions (this work)	70.7	170	286.2

All calculations are based on conservative approximations based on product yield mass found in each report.

Published on 29 July 2021. Downloaded on 4/8/2026 1:39:49 PM.

ChsNC step, in which the scale for Hsieh is on the milligram scale (up to 400 mg product, MI = 920) and our previous work having yield up to 29 g. In the case of the aging method (Table 1, entry 4), performing the second step of the process in the solid-state immediately enabled lower material use. The PMI for the conversion of ChNC to ChsNC has more than 2-fold decrease (PMI = 170) compared to the solvo-thermal method (PMI = 377.7). Importantly, there is drastic reduction in MI when one of the steps is changed in place for a solid-state reaction instead of a "classic" solution-based reaction, where the total MI (from chitin to ChsNCs) is decreased from MI = 494.4 for the solvothermal deacetylation method to MI = 286.2 for the aging deacetylation method. Thus, aging is not only a reliable method to deacetylate ChNCs into ChsNCs, but it is also more sustainable, as evidenced by quantified green metrics.

ChsNC^{Ag} and ChsNCST containing alginate hydrogel rheological study

We then pursued the synthesis of ChsNC-containing hydrogels. For this task, we selected 3-day aged ChsNC^{Ag} (3ChsNC^{Ag}) and 6-day aged ChsNC^{Ag} (6ChsNC^{Ag}) samples as the ones combining high DDA (52.4% and 65.5% resp.), good CrI (40% and 36% resp.), and nanorod morphology, as well as the previously reported ChsNCST (DDA: 88%, CrI: 24% and rod shape), and ChNC (DDA: 0%, CrI: 72% and rod shape).[57] These were combined with sodium alginate which is well known for its ability to form polyelectrolyte complexes (PECs) due to its polyionic nature as well as being biocompatible, lending itself as an attractive hydrogel precursors.[68,69]

Four prototype hydrogels were fabricated using aqueous solutions of 2 wt% Na alginate and aqueous suspensions of 2 wt% ChNC (ChNC-alginate), ChsNCST (ChsNCST-alginate), 3ChsNC^{Ag} (3ChsNC^{Ag}-alginate), or 6ChsNC^{Ag} (6ChsNC^{Ag}-alginate) at pH 5, and subsequently monitored for their rheological behaviour (ESI†). Importantly, no Ca^{2+} ions were used in this setting, unlike most examples of cellulose[70,71] and chitin-based hydrogels,[45] as these cations tend to leach and cause instability during subsequent use. We reasoned that the positive charges in ChsNCs could replace the use of such ions for gelation and afford a more stable material.[53] A 5 mL syringe with 4 wt% sodium alginate solution was combined with another 5 mL syringe with 4 wt% nanocrystal suspension using a syringe connector. It was crucial that the pH was controlled to be pH 5, such that it was below the pK_a value of chitosan (~6.3) and above that of alginate (~3.5).[72] A control test was done in which the gels were made at neutral pH 7, and no gelling occurred. The rheological measurements showed that the use of ChNCs as the crosslinker did not trigger gel formation (Fig. 2a), as seen by the negligible difference between the storage (G') and loss (G'') moduli. In contrast, when ChsNCST was used as the crosslinking agent, the G' was higher than the G'' value, proving that gelation occurred between the alginate and ChsNCs (Fig. 2b), yet with a modest G' value of 12.2 Pa at 1 Hz of shear rate. 3ChsNC^{Ag}-alginate (Fig. 2c) and 6ChsNC^{Ag}-alginate (Fig. 2d) gels showcased superior mechanical properties compared to the ChsNCST-alginate gel, with G' values around 79.2 and 961.7 Pa, respectively, in a gelling time of 2000 s and at 1 Hz of shear rate (Fig. 2e). To sum up, all the tested ChsNC samples were able to crosslink alginate to form gels at pH = 5. These are the first reported hydrogels based on

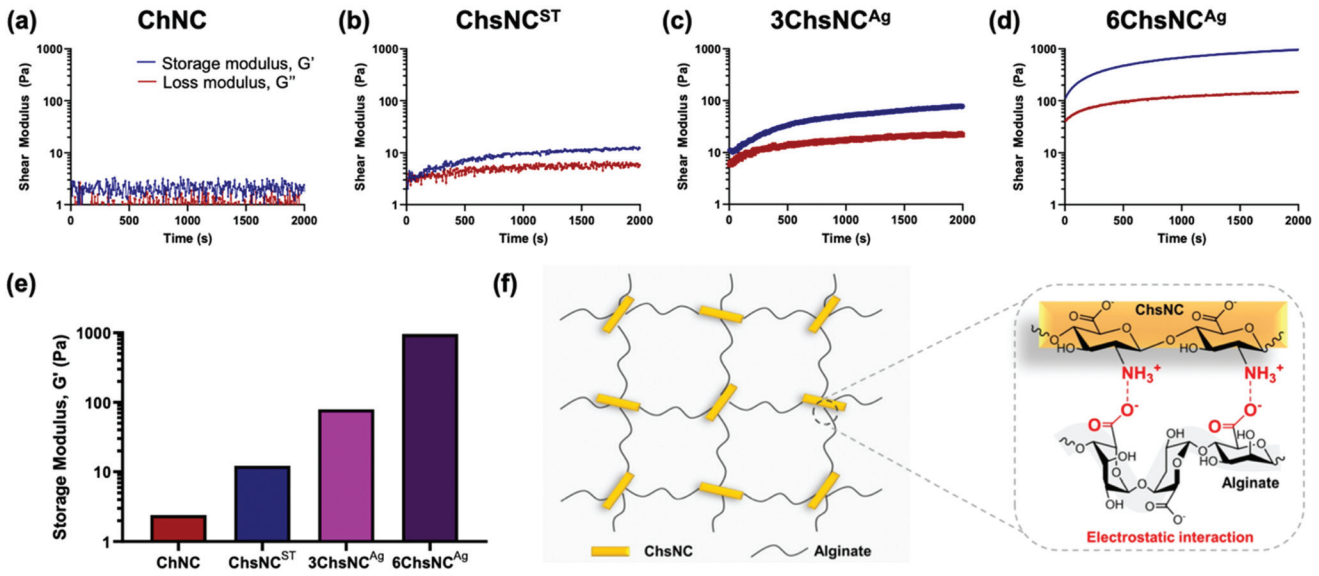

Fig. 2 Rheology measurements for gels made by mixing a 2 wt% Na alginate solution with a suspension of 2 wt% (a) ChNC, (b) ChsNCST, (c) 3ChsNC^{Ag} and (d) 6ChsNC^{Ag} at pH 5. Blue lines depict the storage modulus (G') and red lines show the loss modulus (G''). (e) Storage modulus values at 2000 s for the four gels above. (f) Schematic depicting the crosslinking interaction between the positively-ChsNCs and negatively charged alginate at pH 5.

 This journal is © The Royal Society of Chemistry 2021

Published on 29 July 2021. Downloaded on 4/8/2026 1:39:49 PM.

ChsNCs. In contract, ChNCs were not able to gel with alginates, showcasing the key role of protonated amine functionalities in this context (Fig. 2f). ChsNCST-alginate, 3ChsNC^{Ag}-alginate and 6ChsNC^{Ag}-alginate respectively featured increasing G' values, jumping each time by one order of magnitude. Interestingly, 3ChsNC^{Ag} and 6ChsNC^{Ag} feature very similar CrI and ζ-potential values, while they differ significantly in their DDA values (52.4% and 65.5% resp.). This suggests that this change has a dramatic effect to favour gelation. Interesting, Petrova *et al.* reported an alginate hydrogel made with 30% deacetylated ChNC, and a G' value around 30 Pa at 1 Hz, which is in good agreement with the trend we measured.[53] Interestingly this trend stops when considering ChsNCST, as its high DDA should afford an even better G' value. We propose here that the low CrI of this material imparts too much flexibility, and thus enables phase separation within the ChsNC-alginate gel, as is seen in gels made with bulk chitosan polymer.[73] We did observe visually that no homogeneous macroscopic gel could be formed with this material. These observations suggest that the usage of 6ChsNC^{Ag} as the crosslinker fell in a sweet spot, where the combination of good DDA (65.5%) and still moderate CrI (36%) afforded excellent gelation properties due to successfully arresting microphase separation. The resulting G' value is the highest measured on an Ca^{2+} free alginate gel made with polysaccharide nanocrystals with no surface modification.

Drug release study for ChsNC^{Ag} and ChsNCST containing Ca-alginate hydrogels

To demonstrate the versatility of this system, we decided to test it as a drug release vehicle. Drug delivery with hydrogels has seen extensive research within the past decades.[6] Both alginate[74,75] and nanochitosan[76,77] have been shown in the past to be biocompatible when used as substituents for hydrogels, which bodes well for their use in a combined drug delivery system. Although the gels made above without Ca^{2+} had good properties, they could not retain their integrity upon prolonged exposure to aqueous conditions. In order to provide a more mechanically stable gel for drug delivery, Ca^{2+} cations were introduced as a second crosslinker to form more robust alginate/nanocrystals hydrogel beads. To explore this aspect, bovine serum albumin (BSA) with fluorescein isothiocyanate labelling (BSA-FITC) was chosen as the model protein drug due to its inherent negative charge. BSA is also commonly used as a model negatively charged drug protein, which is often commonly studied such that comparison between our work can be made with previous works.[58,59,78] The hydrogel beads were prepared first by mixing a 4 wt% alginate solution with the nanocrystal solution using a syringe connector and then subsequently added dropwise into 0.2 M $CaCl_2$ (ESI†). Using this method, 5 types of hydrogel beads were fabricated: control hydrogel bead with no nanocrystal incorporation (Ca-alginate), hydrogel beads with 3-day (3ChsNC^{Ag}/Ca-alginate) and 6-day (6ChsNC^{Ag}/Ca-alginate) ChsNC^{Ag} incorporation, hydrogel beads with ChNC incorporation (ChNC/Ca-alginate), and hydrogel beads with ChsNCST incorporation (ChsNCST/Ca-alginate). Swelling ratio experiments were also done without BSA-FITC loading in order to test for the stability of the hydrogel beads (Fig. S7†). All the as-made hydrogel beads held stable for over 8 h with the exception of the hydrogel beads with ChNC incorporation, which lost physical integrity after only 4 h. Furthermore, it was noted that 6ChsNC^{Ag}/Ca-alginate possessed the greatest anti-swelling property out of the 5 hydrogel beads, outperforming the 3ChsNC^{Ag}/Ca-alginate hydrogel bead. Thus, 6ChsNC^{Ag}/Ca-alginate was chosen to be the representative ChsNC^{Ag}-incorporated hydrogel bead to be used for the drug release study.

For loading the BSA-FITC into the hydrogel beads, first a BSA-FITC solution was mixed with the nanocrystal solution and incubated for 1 h to allow for interaction between nanocrystals and proteins. Afterwards, the protein-nanocrystal solution was mixed with alginate, added dropwise into an aqueous 0.2 M $CaCl_2$ bath, and promptly washed quickly three times with D.I. water (ESI†). The drug-loaded beads were then placed in phosphate-buffered saline (PBS) at a pH of 7.4, and the subsequent release profiles were obtained by monitoring 200 μL aliquots at specific time intervals using a micro-well plate reader (Fig. 3a–c).

It was observed that ChsNC^{Ag}/Ca-alginate, ChNC/Ca-alginate and the control Ca-alginate hydrogel beads all featured a comparable drug release profile, with about 70% of the drug being released after only 10 h (Fig. 3a and b). These results indicate prolonged release in agreement with past reports on calcium-crosslinked alginate-based systems.[59,79] Interestingly, the release rate was significantly lower in the ChsNCST-Ca-alginate system, as only 20% of the drug was released after 10 hours and 55% after 3 days. The half-life time, which is the time at which 50% of the loaded BSA-FITC has been released, was plotted by qualitatively interpolating the points within the release profile (Fig. 3c). Surprisingly, it is seen that almost an order of magnitude increase in the half-life time is achieved with the ChsNCST/Ca-alginate system in comparison with the other systems. Intrigued by this phenomenon, we investigated whether this could be due to the phase separation that was happening within the ChsNCST/Ca-alginate system, which can be seen in the optical photographs of the hydrogel beads (Fig. 3d–g). The control Ca-hydrogel beads (Fig. 3d) were clear, while the 6ChsNC^{Ag}/Ca-alginate (Fig. 3e) and ChNC/Ca-alginate (Fig. 3f) hydrogel beads were translucent but still homogeneous. However, the ChsNCST/Ca-alginate beads depict clear inhomogeneity within the matrix, indicative of phase separation of the BSA-FITC within the gel (Fig. 3g). To explore this further, we employed the use of confocal microscopy (Fig. 3h–k). The control Ca-alginate beads show uniform brightness (Fig. 3h) while the 6ChsNC^{Ag}/Ca-alginate beads have distinct bright spots, indicative of small sites of interaction between the BSA and 6ChsNC^{Ag} (Fig. 3i). With ChNC incorporation, there are no bright spots and only dark sites which indicate no interaction is occurring between the ChNC and BSA-FITC (Fig. 3j). Yet, one can see the clear contrast when ChsNCST is used as the substituent in the Ca-alginate gel (Fig. 3k), which is seen to have a 3-D network within the hydrogel bead. This is

Published on 29 July 2021. Downloaded on 4/8/2026 1:39:49 PM.

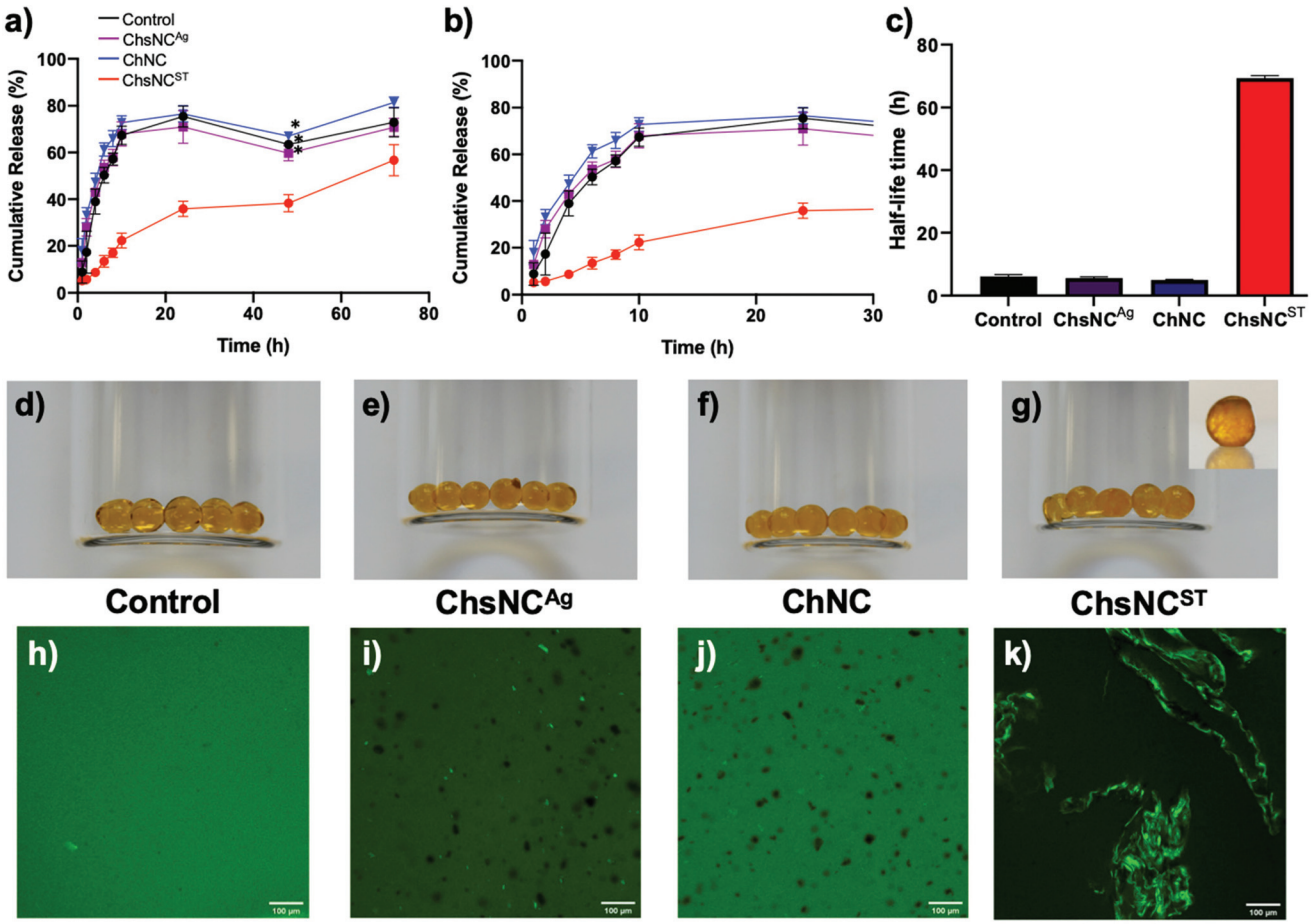

Fig. 3 (a) Release profiles for control (Ca-alginate), ChsNC^{Ag} (6ChsNC^{Ag}/Ca-alginate), ChNC (ChNC/Ca-alginate), and ChsNCST (ChsNCST/Ca-alginate) hydrogel beads with BSA-FITC incorporation over the course of 72 h. *The decrease in cumulative drug release at 48 h is due to experimental error, and can be accounted for by the error bars. (b) Expanded view for the initial 24 h release profile. The legend for figure (a) is the same for (b). (c) Bar graph depicting the half-life time values for cumulative BSA-FITC release from the above-mentioned BSA-FITC loaded alginate gels. (d–g) Optical photographs of the respective BSA-FITC loaded hydrogel beads, inset of (g) is a photograph of the same sample at a higher magnification. (h–k) Confocal microscopy images of the respective BSA-FITC loaded hydrogel beads.

also evidence that supports the hypothesis of phase separation occurring between the ChsNCST and alginate, further verified by the low modulus values (Fig. 2b). In combination with both the formation of condensed ChsNCST-alginate phases, as well as the BSA-FITC being incorporated into this phase (due to the BSA-FITC being initially loaded with the ChsNCs), the high crosslinking density of the resulting matrix resulted in remarkably sustained drug release. In summary, it can be concluded that it is not the morphological aspect (*i.e.*, the length and width of the nanorod) that matters in the ability to retain the drug for the resulting nanocrystal-incorporated hydrogel, but in fact the crystallinity and DDA of the ChsNCs itself. The key comparison is made between the Ca^{2+}-alginate hydrogels with 6-day aged ChsNC^{Ag} (CrI = 36%, DDA = 65%) and ChsNCST (CrI = 24%, DDA = 88%) incorporation (Fig. 3a). While the length of the two types of ChsNCs were relatively similar (6-day aged ChsNC^{Ag} = 203 nm, ChsNCST = 182 nm), the resulting hydrogels had substantially different release profiles. We reason that since the ChsNCST has higher DDA, and therefore more amines to interact with the protein, as well as being more "flexible" in accordance with having low CrI, it can bind better to the BSA and therefore slow down the drug release. This preferential binding is also seen in the confocal microscopy of the ChsNCST/Ca-alginate (Fig. 3k), where clear phase separation is evidenced in contrast to the 6ChsNC^{Ag}/Ca-alginate gel.

In comparison with bulk chitosan, Chen *et al.* used bulk carboxymethyl chitosan blended with alginate and cross-linked with genipen to create a hydrogel for release of BSA. In their report, they provided a release of 80% cumulative drug release within the first 5 hours at pH 7.4.[59] While, other gel systems with biopolymer incorporation such as methylcellulose also had rapid cumulative BSA release of at least 70% within the first 6 h at pH 7.4.[58] It can be seen that for these systems, the nanoscale attributes of the ChsNC such as crystallinity and DDA plays a crucial role in determining the properties seen at the macroscale, which we can uniquely tailor using this family of nanocrystals.

 This journal is © The Royal Society of Chemistry 2021

Published on 29 July 2021. Downloaded on 4/8/2026 1:39:49 PM.

Conclusions

A novel and sustainable aging methodology was utilized to synthesize ChsNCs from ChNCs. The as-made ChsNC^{Ag} had higher DDA values as compared to those in the literature, while also retaining moderate crystallinity, as seen through pXRD. Retention of its nano-rod morphology was visualized through TEM. Sustainability metrics were assessed for the first time for the transformation of chitin to ChsNCs, and the value of solid-state aging verified to have a significant impact in lowering the PMI of the process. The application of this family of ChsNCs with varying properties to hydrogel formation and drug release was explored for the first time. We validated the ability of ChsNC^{Ag} and ChsNCST to gel with negatively charged alginate. Compelling results demonstrated that the higher crystallinity in ChsNC^{Ag} was key in strengthening the mechanical properties of alginate hydrogels. Finally, the ChsNC^{Ag} and ChsNCST were incorporated within a Ca^{2+}-mediated alginate gel system in order to test their ability to provide sustained drug release of the model protein drug BSA-FITC. ChsNCST featured a much more sustained drug release profile, which outcompetes systems using both bulk chitosan as well as bulk cellulose, further emphasizing the imperative role anime groups and nanostructure plays in these materials. These results demonstrate that tunability of nanocrystals chemical, structural and physical properties is absolutely crucial in order to tailor the material to the needs of hydrogel formation, stabilization, and biomedical application. Herein, we showcase a very simple and clean method to generate a family of ChsNC-based materials with desirable tunability and outstanding properties for both hydrogel formation and sustaining drug release.

Conflicts of interest

All the authors declare no conflicts of interest.

Acknowledgements

We thank the Natural Science and Engineering Research Council of Canada (NSERC) Discovery Grant, Discovery Accelerator Supplement [AM], and Postgraduate Scholarship-Doctoral award,[5] the Canada Foundation for Innovation (CFI), the Canada Research Chair program [VKM, JL], New Frontiers in Research Fund - Exploration, the Fonds de Recherche du Quebec – Nature et Technology (FRQNT) – Centre for Green Chemistry and Catalysis (CGCC), McGill University and NRC Industrial Biotechnology program [EL] for their financial support. We are grateful to Dr Robin Stein for scientific discussion and to Dr Hatem Titi for his help in acquiring the pXRD data.

References

1 K. Y. Lee and D. J. Mooney, *Chem. Rev.*, 2001, **101**, 1869–1880.
2 D. J. Beebe, J. S. Moore, J. M. Bauer, Q. Yu, R. H. Liu, C. Devadoss and B.-H. Jo, *Nature*, 2000, **404**, 588–590.
3 J. Li, A. D. Celiz, J. Yang, Q. Yang, I. Wamala, W. Whyte, B. R. Seo, N. V. Vasilyev, J. J. Vlassak, Z. Suo and D. J. Mooney, *Science*, 2017, **357**, 378–381.
4 B. Qu and Y. Luo, *Int. J. Biol. Macromol.*, 2020, **152**, 437–448.
5 A. Döring, W. Birnbaum and D. Kuckling, *Chem. Soc. Rev.*, 2013, **42**, 7391–7420.
6 J. Li and D. J. Mooney, *Nat. Rev. Mater.*, 2016, **1**, 1–17.
7 D. M. R. Gibbs, C. R. M. Black, J. I. Dawson and R. O. C. Oreffo, *J. Tissue Eng. Regener. Med.*, 2016, **10**, 187–198.
8 E. M. Ahmed, *J. Adv. Res.*, 2015, **6**, 105–121.
9 K. J. De France, T. Hoare and E. D. Cranston, *Chem. Mater.*, 2017, **29**, 4609–4631.
10 R. Parhi, *Adv. Pharm. Bull.*, 2017, **7**, 515–530.
11 L. Liu, L. Bai, A. Tripathi, J. Yu, Z. Wang, M. Borghei, Y. Fan and O. J. Rojas, *ACS Nano*, 2019, **13**, 2927–2935.
12 R. Grande, L. Bai, L. Wang, W. Xiang, O. Ikkala, A. J. F. Carvalho and O. J. Rojas, *ACS Sustainable Chem. Eng.*, 2020, **8**, 1137–1145.
13 L. Heath, L. Zhu and W. Thielemans, *ChemSusChem*, 2013, **6**, 537–544.
14 V. G. Muir and J. A. Burdick, *Chem. Rev.*, 2020, DOI: 10.1021/acs.chemrev.0c00923.
15 S.-K. Kim, *Chitin, chitosan, oligosaccharides and their derivatives: biological activities and applications*, CRC Press, 2010.
16 M. N. V. R. Kumar, R. A. A. Muzzarelli, C. Muzzarelli, H. Sashiwa and A. J. Domb, *Chem. Rev.*, 2004, **104**, 6017–6084.
17 T. A. Khan, K. K. Peh and H. S. Ch'ng, *J. Pharm. Pharm. Sci.*, 2002, **5**, 205–212.
18 B. Luppi, F. Bigucci, A. Abruzzo, G. Corace, T. Cerchiara and V. Zecchi, *Eur. J. Pharm. Biopharm.*, 2010, **75**, 381–387.
19 N. Sudarshan, D. Hoover and D. Knorr, *Food Biotechnol.*, 1992, **6**, 257–272.
20 X. F. Liu, Y. L. Guan, D. Z. Yang, Z. Li and K. D. Yao, *J. Appl. Polym. Sci.*, 2001, **79**, 1324–1335.
21 A. Baranwal, A. Kumar, A. Priyadharshini, G. S. Oggu, I. Bhatnagar, A. Srivastava and P. Chandra, *Int. J. Biol. Macromol.*, 2018, **110**, 110–123.
22 C. Peniche, W. Argüelles-Monal and F. M. Goycoolea, in *Monomers, Polymers and Composites from Renewable Resources*, ed. M. N. Belgacem and A. Gandini, Elsevier, Amsterdam, 2008, pp. 517–542, DOI: 10.1016/B978-0-08-045316-3.00025-9.
23 F. M. Kerton, Y. Liu, K. W. Omari and K. Hawboldt, *Green Chem.*, 2013, **15**, 860–871.
24 N. Yan and X. Chen, *Nature*, 2015, **524**, 155–157.

Published on 29 July 2021. Downloaded on 4/8/2026 1:39:49 PM.

25 H. Yang and N. Yan, in *Green Chemistry and Chemical Engineering*, ed. B. Han and T. Wu, Springer New York, New York, NY, 2019, pp. 461–482, DOI: 10.1007/978-1-4939-9060-3_1012.
26 H. K. No and E. Y. Hur, *J. Agric. Food Chem.*, 1998, **46**, 3844–3846.
27 M. J. Hülsey, *Green Energy Environ.*, 2018, **3**, 318–327.
28 F. M. Kerton and N. Yan, *Fuels, Chemicals and Materials from the Oceans and Aquatic Sources*, John Wiley & Sons, 2017.
29 C. Hadad, E. Husson and A. N. Van Nhien, in *Encyclopedia of Ionic Liquids*, Springer, Singapore, 2020, pp. 1–6.
30 R. Devi and R. Dhamodharan, *ACS Sustainable Chem. Eng.*, 2018, **6**, 846–853.
31 J. P. D. Therien, F. Hammerer, T. Friščić and K. Auclair, *ChemSusChem*, 2019, **12**, 3481–3490.
32 T. Maschmeyer, R. Luque and M. Selva, *Chem. Soc. Rev.*, 2020, **49**, 4527–4563.
33 T. Di Nardo, C. Hadad, A. N. Van Nhien and A. Moores, *Green Chem.*, 2019, **21**, 3276–3285.
34 X. Chen, H. Yang, Z. Zhong and N. Yan, *Green Chem.*, 2017, **19**, 2783–2792.
35 D. Klemm, F. Kramer, S. Moritz, T. Lindström, M. Ankerfors, D. Gray and A. Dorris, *Angew. Chem., Int. Ed.*, 2011, **50**, 5438–5466.
36 X. M. Dong, J.-F. Revol and D. G. Gray, *Cellulose*, 1998, **5**, 19–32.
37 R. Marchessault, F. Morehead and N. Walter, *Nature*, 1959, **184**, 632–633.
38 J. Li, J. Revol and R. Marchessault, *J. Colloid Interface Sci.*, 1996, **183**, 365–373.
39 Y. Fan, T. Saito and A. Isogai, *Carbohydr. Polym.*, 2010, **79**, 1046–1051.
40 Y. Fan, T. Saito and A. Isogai, *Biomacromolecules*, 2008, **9**, 192–198.
41 B. Thomas, M. C. Raj, K. B. Athira, M. H. Rubiyah, J. Joy, A. Moores, G. L. Drisko and C. Sanchez, *Chem. Rev.*, 2018, **118**, 11575–11625.
42 N. Lin and A. Dufresne, *Eur. Polym. J.*, 2014, **59**, 302–325.
43 M. Kaushik and A. Moores, *Green Chem.*, 2016, **18**, 622–637.
44 M. Liu, J. Huang, B. Luo and C. Zhou, *Int. J. Biol. Macromol.*, 2015, **78**, 23–31.
45 Y. Huang, M. Yao, X. Zheng, X. Liang, X. Su, Y. Zhang, A. Lu and L. Zhang, *Biomacromolecules*, 2015, **16**, 3499–3507.
46 S. Sultan and A. P. Mathew, *Nanoscale*, 2018, **10**, 4421–4431.
47 H. Kargarzadeh, R. M. Sheltami, I. Ahmad, I. Abdullah and A. Dufresne, *Polymer*, 2015, **56**, 346–357.
48 W. J. Lee, A. J. Clancy, E. Kontturi, A. Bismarck and M. S. P. Shaffer, *ACS Appl. Mater. Interfaces*, 2016, **8**, 31500–31504.
49 K. Song, W. Zhu, X. Li and Z. Yu, *Mater. Lett.*, 2020, **260**, 126884.
50 J. Yang, J.-J. Zhao, C.-R. Han, J.-F. Duan, F. Xu and R.-C. Sun, *Cellulose*, 2014, **21**, 541–551.
51 R. Nigmatullin, R. Harniman, V. Gabrielli, J. C. Muñoz-García, Y. Z. Khimyak, J. Angulo and S. J. Eichhorn, *ACS Appl. Mater. Interfaces*, 2018, **10**, 19318–19322.
52 N. Lin, A. Gèze, D. Wouessidjewe, J. Huang and A. Dufresne, *ACS Appl. Mater. Interfaces*, 2016, **8**, 6880–6889.
53 V. A. Petrova, V. Y. Elokhovskiy, S. V. Raik, D. N. Poshina, D. P. Romanov and Y. A. Skorik, *Biomolecules*, 2019, **9**, 291.
54 S. Phongying, S.-I. Aiba and S. Chirachanchai, *Polymer*, 2007, **48**, 393–400.
55 A. G. Pereira, E. C. Muniz and Y.-L. Hsieh, *Carbohydr. Polym.*, 2014, **107**, 158–166.
56 A. G. Pereira, E. C. Muniz and Y.-L. Hsieh, *Carbohydr. Polym.*, 2015, **123**, 46–52.
57 T. Jin, D. Kurdyla, S. Hrapovic, A. C. W. Leung, S. Régnier, Y. Liu, A. Moores and E. Lam, *Biomacromolecules*, 2020, **21**, 2236–2245.
58 H.-F. Liang, M.-H. Hong, R.-M. Ho, C.-K. Chung, Y.-H. Lin, C.-H. Chen and H.-W. Sung, *Biomacromolecules*, 2004, **5**, 1917–1925.
59 S.-C. Chen, Y.-C. Wu, F.-L. Mi, Y.-H. Lin, L.-C. Yu and H.-W. Sung, *J. Controlled Release*, 2004, **96**, 285–300.
60 G. Margoutidis, V. H. Parsons, C. S. Bottaro, N. Yan and F. M. Kerton, *ACS Sustainable Chem. Eng.*, 2018, **6**, 1662–1669.
61 M. Yabushita, H. Kobayashi, K. Kuroki, S. Ito and A. Fukuoka, *ChemSusChem*, 2015, **8**, 3760–3763.
62 A. Y. Li, A. Segalla, C.-J. Li and A. Moores, *ACS Sustainable Chem. Eng.*, 2017, **5**, 11752–11760.
63 M. Y. Malca, P.-O. Ferko, T. Friščić and A. Moores, *Beilstein J. Org. Chem.*, 2017, **13**, 1963–1968.
64 T. Di Nardo and A. Moores, *Beilstein J. Org. Chem.*, 2019, **15**, 1217–1225.
65 L. Raymond, F. G. Morin and R. H. Marchessault, *Carbohydr. Res.*, 1993, **246**, 331–336.
66 Y. Zhang, C. Xue, Y. Xue, R. Gao and X. Zhang, *Carbohydr. Res.*, 2005, **340**, 1914–1917.
67 D. P. Debecker, K. Kuok Hii, A. Moores, L. M. Rossi, B. Sels, D. T. Allen and B. Subramaniam, *ACS Sustainable Chem. Eng.*, 2021, **9**, 4936–4940.
68 H. V. Sæther, H. K. Holme, G. Maurstad, O. Smidsrød and B. T. Stokke, *Carbohydr. Polym.*, 2008, **74**, 813–821.
69 W. H. Tan and S. Takeuchi, *Adv. Mater.*, 2007, **19**, 2696–2701.
70 N. Mohammed, N. Grishkewich, R. M. Berry and K. C. Tam, *Cellulose*, 2015, **22**, 3725–3738.
71 J. Supramaniam, R. Adnan, N. H. Mohd Kaus and R. Bushra, *Int. J. Biol. Macromol.*, 2018, **118**, 640–648.
72 F. Gu, B. Amsden and R. Neufeld, *J. Controlled Release*, 2004, **96**, 463–472.
73 M.-S. Shin, S. J. Kim, S. J. Park, Y. H. Lee and S. I. Kim, *J. Appl. Polym. Sci.*, 2002, **86**, 498–503.
74 M. C. Darnell, J.-Y. Sun, M. Mehta, C. Johnson, P. R. Arany, Z. Suo and D. J. Mooney, *Biomaterials*, 2013, **34**, 8042–8048.
75 O. Smidsrød and G. Skjåk-Br┤k, *Trends Biotechnol.*, 1990, **8**, 71–78.

 This journal is © The Royal Society of Chemistry 2021

76 G. Thandapani, P. Supriya Prasad, P. N. Sudha and A. Sukumaran, *Int. J. Biol. Macromol.*, 2017, **104**, 1794–1806.
77 S. Rodrigues, M. Dionísio, C. R. López and A. Grenha, *J. Funct. Biomater.*, 2012, **3**, 615–641.
78 M. Ghaemy and M. Naseri, *Carbohydr. Polym.*, 2012, **90**, 1265–1272.
79 L.-S. Liu, S.-Q. Liu, S. Y. Ng, M. Froix, T. Ohno and J. Heller, *J. Controlled Release*, 1997, **43**, 65–74.

Published on 29 July 2021. Downloaded on 4/8/2026 1:39:49 PM.